Computing the CMB power spectrum

Iván Villegas Pérez⋆ 🆔

High Energy Physics (HEP) Section, Department of Physics, University of Oslo, Sem Sælands vei 24,0371 Oslo, Norway
e-mail: ivanvi@uio.no

May 29, 2024

ABSTRACT

Context. The goal of this whole study is to be able to predict the CMB (and matter) fluctuations (described by the so-called power-spectrum) from first principles and learn about all the different physical processes that goes on to be able to explain the results.
Aims. The goals in this work are to make a class/module that takes in the cosmological parameters and has functions for getting the Hubble parameter, conformal time and distance measures as function of scale factor and the variable $x = \ln a$, to make a class/module that takes in the abundance of Helium in the Universe and has functions for getting the free electron fraction, the optical depth (and its derivatives) and the visibility function (and its derivatives), to make a class/module that evolves the density, velocity, temperature, polarization and neutrinos perturbations from an early time until today, and to make a class/module that computes the CMB power-spectrum.
Methods. Four codes have been developed, using the template given by Hans A. Winther. In the first code, several functions have been implemented to solve the background cosmology of the Universe and plot the results, identifying each epoch domination (either relativistic particles, non-relativistic matter or dark energy). In the second code, several functions have been implemented to solve the recombination history of the Universe and plot the results. In the third one, several functions have been implemented to evolve the perturbations and plot the results. Lastly, in the fourth code, several functions have been implemented to compute the CMB power-spectrum and plot the results.
Results. Background cosmology of the Universe has been solved and each epoch has been determined, identifying in each of them the dominating substance. The age of the Universe has also been computed, being this $t_{\text{Universe}} \approx 13.86$ Gyr. Recombination history of the Universe has been solved. The relevant times of the Universe's recombination history have been computed, as well as the sound horizon at decoupling, being this $r_s \approx 128.177$ Mpc. Evolution of the structure of the Universe has been solved. The density and velocity perturbations for CDM, baryonic matter and photon have been computed. The CMB power-spectrum has been computed, along with a CMB map.
Conclusions. The CMB power-spectrum has been computed with a high accuracy, considering the approximations made except for the low ℓ's, where some mistake in the Doppler component of the source function has given discrepancies with the observational data.

Key words. background cosmology – evolution of the Universe – epoch domination – recombination – structure evolution – perturbations – CMB power-spectrum – CMB map

1. Introduction

The goals of this study have been to solve the evolution of the uniform background cosmology in the Universe, to solve its recombination history, to solve the evolution of structure in the Universe and to compute the CMB power-spectrum.[1]

For this first goal, a class/module has been implemented. This class takes the given cosmological parameters sand (with the use of different functions) returns the Hubble parameter (H), conformal time (η) and distance measures as function of the scale factor (a) and the variable x ($x = \ln a$), which will be the main time variable for this work.[2]

For the second goal, a different class/module has been implemented. The final goal of this part is to compute the optical depth (τ) as a function of x and its derivatives, and the visibility function, $\tilde{g}$, and its derivatives.[3]

For the third goal, a different class/module has been implemented. The final goal of this part is to construct two-dimensional functions (of time and Fourier scale, x and k) for each of the main physical quantities of interest: $\Phi(x,k)$, $\Psi(x,k)$, $\delta_{\text{CDM}}(x,k)$, $\delta_b(x,k)$, $v_{\text{CDM}}(x,k)$, $v_B(x,k)$ and $\Theta_\ell(x,k)$.[4]

Finally, after spending a lot of time on understanding the evolution of the background properties of the universe, its ionization history, and the growth of structure in the universe, the key statistical observable in cosmology has been computed: the CMB and matter power spectrum![5]

The fiducial cosmology used in this work is the best-fit cosmology found from fits to Planck 2018 data [Aghanim et al. (2020)] without photon polarization, neutrinos oscillations, reionization nor Helium:

⋆ GitHub: https://github.com/ivanvillegas7/CMB_power_spectrum
Orcid: https://orcid.org/0009-0001-2300-603X
[1] Hans A. Winther, Cosmology II: A numerical project on the formation of the CMB and structures in the Universe: https://cmb.wintherscoming.no/index.php
[2] Milestone I: Background Cosmology

[3] Milestone II: Recombination History
[4] Milestone III: Evolution of structure in the Universe
[5] Milestone IV: The CMB and matter power-spectra

$$h_0 = 0.67,$$

$$T_{\text{CMB},0} = 2.7255 \text{ K},$$

$$N_{\text{eff}} = 3.046,$$

$$\Omega_{\text{B},0} = 0.05,$$

$$\Omega_{\text{CDM},0} = 0.267,$$

$$\Omega_{k,0} = -\frac{kc^2}{H_0^2} = 0,$$

$$\Omega_{\Lambda,0} = 1 - (\Omega_{\text{B},0} + \Omega_{\text{CDM},0} + \Omega_{k,0} + \Omega_{\nu,0} + \Omega_{\gamma,0}),$$

$$Y_p = 0,$$

$$z_{\text{reion}} = 0,$$

$$\Delta z_{\text{reion}} = 0,$$

$$z_{\text{He, reion}} = 0,$$

$$\Delta z_{\text{He, reion}} = 0,$$

$$n_s = 0.965,$$

$$A_s = 2.1 \cdot 10^{-9}.$$

Each quantity will be explained in the following section.

2. Basic cosmology

2.1. Background Cosmology

Lets review the theory basics. The goal of this work has been computing the expansion history of the universe, and look at the uniform background densities of the various matter and energy components. Lets first define the Friedmann-Lemaître-Robertson-Walker metric (here for a flat space where $k = 0$),

$$ds^2 = -c^2 dt^2 + a^2(t) \left[dr^2 + r^2 \left(d\theta^2 + \sin^2\theta d\phi^2 \right) \right], \quad (1)$$

or in Cartesian coordinates

$$ds^2 = a^2(t) \left(d\eta^2 + dx^2 + dy^2 + dz^2 \right), \quad (2)$$

where $a(t)$ is the scale factor, which measures the size of the universe relative to today ($a_0 = a_{\text{today}} = 1$), and η is called conformal time. One thing to note: it is called conformal time, but it is usually given in units of length for it to have the same dimension as the spatial coordinates. The conversion factor for this is the speed of light (c). In this work the conformal time is a distance (and the corresponding time is this distance divided by the speed of light). As we will be looking at phenomena that varies strongly over a wide range of time scales, we will mostly be using the logarithm of the scale factor, $x \equiv \ln a$, as the main time variable. A fifth time variable is the redshift, z, which is defined as

$$1 + z = a_0/a(t) \quad (3)$$

Einstein's General Relativity describes how the metric evolves with time, given some matter and density components.

The relevant equation for this work purposes is the Friedmann equation, which may be written (when $k = 0$ is not assumed) on the following form

$$H = H_0 \sqrt{\Omega_{\text{M},0} a^{-3} + \Omega_{\text{R},0} a^{-4} + \Omega_{k,0} a^{-2} + \Omega_{\Lambda,0}}, \quad (4)$$

where $H \equiv \dot{a}/a$ is the Hubble parameter (dot denotes derivatives with respect to physical time, $\dot{} = d/dt$), and $\Omega_{\text{B},0}$, $\Omega_{\text{CDM},0}$, $\Omega_{\gamma,0}$, $\Omega_{\nu,0}$, and $\Omega_{\Lambda,0}$ are the present day relative densities of baryonic (ordinary) matter, dark matter, radiation, neutrinos and dark energy, respectively. A subscript 0 denotes the value at the present time. The terms $\Omega_{\text{M},0} = \Omega_{\text{B},0} + \Omega_{\text{CDM},0}$ and $\Omega_{\text{R},0} = \Omega_{\nu,0} + \Omega_{\gamma,0}$, stand for cold (non-relativistic) matter and relativistic particles (neutrinos and photons). The term $\Omega_{k,0}$ denotes curvature and acts in the Friedmann equation as if it were a normal matter fluid with equation of state $\omega = -1/3$. This term follows from the other density parameters which can be seen from taking $a = 1$ to get $\Omega_{k,0} = 1 - \Omega_{\text{M},0} - \Omega_{\text{R},0} - \Omega_{\Lambda,0}$. A scaled Hubble parameter, $\mathcal{H} \equiv aH$, is has also been introduced. In this work, curvature has only been implemented when it comes to solving the cosmological background and the fiducial cosmology has $\Omega_k = 0$.

The Friedmann equations also describe how each component evolve with time

$$\dot{\rho} + 3H(\rho + P) = 0 \quad (5)$$

where P is the pressure. It is useful to define the equation of state $\omega \equiv P/\rho$ (which has been considered constant for the fluids considered in this work). In terms of this, the solution reads $\rho \propto a^{-3(1+\omega)}$. For non-relativistic matter we have $\omega = 0$, for relativistic particles we have $\omega = 1/3$ and for a cosmological constant (Λ) we have $\omega = -1$. This gives us:

$$\rho_{\text{CDM}} = \rho_{\text{CDM},0} a^{-3} \quad (6)$$

$$\rho_{\text{B}} = \rho_{\text{B},0} a^{-3} \quad (7)$$

$$\rho_{\gamma} = \rho_{\gamma,0} a^{-4} \quad (8)$$

$$\rho_{\nu} = \rho_{\nu,0} a^{-4} \quad (9)$$

$$\rho_{\Lambda} = \rho_{\Lambda,0} \quad (10)$$

Here, quantities with subscripts 0 indicate today's values. The density parameters $\Omega_X(a) = \rho_X/\rho_c$ can be written

$$\Omega_k(a) = \frac{\Omega_{k,0}}{a^2 H^2(a)/H_0^2}, \tag{11}$$

$$\Omega_{\mathrm{CDM}}(a) = \frac{\Omega_{\mathrm{CDM},0}}{a^3 H^2(a)/H_0^2}, \tag{12}$$

$$\Omega_{\mathrm{B}}(a) = \frac{\Omega_{\mathrm{B},0}}{a^3 H^2(a)/H_0^2}, \tag{13}$$

$$\Omega_\gamma(a) = \frac{\Omega_{\gamma,0}}{a^4 H^2(a)/H_0^2}, \tag{14}$$

$$\Omega_\nu(a) = \frac{\Omega_{\nu,0}}{a^4 H^2(a)/H_0^2}, \tag{15}$$

$$\Omega_\Lambda(a) = \frac{\Omega_{\Lambda,0}}{H^2(a)/H_0^2}. \tag{16}$$

Two of the density parameters above follows from the observed temperature of the CMB. we have that $\Omega_{\gamma,0}$ and $\Omega_{\nu,0}$ are given by

$$\Omega_{\gamma,0} = 2 \cdot \frac{\pi^2}{30} \frac{(k_B T_{\mathrm{CMB},0})^4}{\hbar^3 c^5} \cdot \frac{8\pi G}{3H_0^2}, \tag{17}$$

$$\Omega_{\nu,0} = N_{\mathrm{eff}} \cdot \frac{7}{8} \left(\frac{4}{11}\right)^{4/3} \Omega_{\gamma,0}, \tag{18}$$

where $T_{\mathrm{CMB},0} = 2.7255\mathrm{K}$ is the temperature of the CMB today and $N_{\mathrm{eff}} = 3.046$ is the effective number of massless neutrinos (slightly larger than 3 due to the fact that neutrinos had not completely decoupled when electrons and positrons annihilate and the 0.046 accounts for the extra energy pumped into the neutrinos). We define matter-radiation equality as the time when $\Omega_{\mathrm{M}} = \Omega_{\mathrm{R}}$ and the matter-dark energy transition as the time when $\Omega_{\mathrm{M}} = \Omega_\Lambda$. The onset of acceleration is the time when $\ddot{a} = 0$.

Another crucial concept for CMB computations is that of the *horizon*. This is simply the distance that light may have travelled since the Big Bang, $t = 0$. If the universe was static, this would simply have been ct, but since the universe also expands, it will be somewhat larger. Note that the horizon is a strictly increasing quantity with time, and we can therefore use it as a time variable. This is often called *conformal time*, and is denoted η.

To find a computable expression for η, note that

$$\frac{\mathrm{d}\eta}{\mathrm{d}t} = \frac{c}{a}. \tag{19}$$

The left-hand side of this equation may be written into

$$\frac{\mathrm{d}\eta}{\mathrm{d}t} = \frac{\mathrm{d}\eta}{\mathrm{d}a}\frac{\mathrm{d}\eta}{\mathrm{d}a} = \frac{\mathrm{d}\eta}{\mathrm{d}a} aH, \tag{20}$$

such that

$$\frac{\mathrm{d}\eta}{\mathrm{d}a} = \frac{c}{a^2 H} = \frac{c}{a\mathcal{H}}, \tag{21}$$

and

$$\frac{\mathrm{d}\eta}{\mathrm{d}x} = \frac{\mathrm{d}a}{\mathrm{d}x}\frac{\mathrm{d}\eta}{\mathrm{d}a} = \frac{c}{\mathcal{H}}. \tag{22}$$

This is a differential equation for η, that can either be solved numerically by direct integration, or by plugging the expression into a ordinary differential equation solver. The initial condition is $\eta(-\infty) = 0$. We cannot integrate from $-\infty$ so, in practice, we pick some very early time x_{start} and use the analytical approximation

$$\eta(x_{\mathrm{start}}) = \frac{c}{\mathcal{H}(x_{\mathrm{start}})}. \tag{23}$$

Some distance measures have also been needed. Considering the line-element in spherical coordinates

$$\mathrm{d}s^2 = -c^2\mathrm{d}t^2 + a^2\left(\frac{\mathrm{d}r^2}{1-kr^2} + r^2\mathrm{d}\theta^2 + r^2\sin^2\theta\mathrm{d}\phi^2\right). \tag{24}$$

Photons move on 0-geodesics, $\mathrm{d}s^2 = 0$, so, considering a radially moving photon ($\mathrm{d}\theta = \mathrm{d}\phi = 0$) traveling from (t,r) to us today at $(t = t_{\mathrm{today}}, r = 0)$, we get

$$c\mathrm{d}t = \frac{a\mathrm{d}r}{\sqrt{1-kr}} \implies \int_t^{t_{\mathrm{today}}} \frac{c\mathrm{d}t}{a} = \int_0^r \frac{\mathrm{d}r'}{\sqrt{1-kr'}}. \tag{25}$$

The left hand side is called the co-moving distance and is closely related to the conformal time

$$\chi = \eta_0 - \eta \tag{26}$$

Evaluating the integral on the right, the full equation above can then be written as

$$
r = \begin{cases} \chi \dfrac{\sin\left(\sqrt{|\Omega_{k,0}|}H_0\chi/c\right)}{\sqrt{|\Omega_{k,0}|}H_0\chi/c} & if \quad \Omega_{k,0} < 0 \\[2ex] \chi & if \quad \Omega_{k,0} = 0 \\[2ex] \chi \dfrac{\sinh\left(\sqrt{|\Omega_{k,0}|}H_0\chi/c\right)}{\sqrt{|\Omega_{k,0}|}H_0\chi/c} & if \quad \Omega_{k,0} > 0 \end{cases} \tag{27}
$$

For a flat Universe, we simply have $r = \chi = \eta_0 - \eta$. With this in hand, all the standard distance measures we have in cosmology can be computed. Knowing an object's physical size, D, and its angular size, θ, as viewed from earth then, the angular diameter distance is defined as $d_A = D/\theta$. From the line-element it can be seen that the angular distance when moving in the θ-direction is $dD = ard\theta$ so

$$
d_A = \frac{D}{\theta} = ar. \tag{28}
$$

Note that for a flat Universe the angular diameter distance reduces to $d_A = a\chi = a \cdot (\eta_0 - \eta)$. The last distance needed is the luminosity distance. Knowing the intrinsic luminosity of a source and measure its flux then we can define the distance to the source via $F = L/4\pi d_L^2$, which is simply

$$
d_L = \frac{r}{a} = \frac{d_A}{a^2}. \tag{29}
$$

It can be seen that all distance measures are given directly from the conformal time, the scale-factor and the curvature.

Finally, the relation between cosmic time t and the time-coordinate x. From $H = \frac{1}{a}\frac{da}{dt} \rightarrow dt = \frac{da}{aH}$ it can be derived that

$$
t(x) = \int_0^a \frac{da}{aH} = \int_{-\infty}^x \frac{dx}{H(x)}. \tag{30}
$$

This can be solved as for η, evolving the ODE[6]

$$
\frac{dt}{dx} = \frac{1}{H}. \tag{31}
$$

In the radiation domination era it can be expressed as $t(x) = 1/2H(x)$, so the initial condition is $t(x_{\text{start}}) = 1/2H(x_{\text{start}})$. Evaluating this at $x = 0$ (today) the age of the Universe can be computed.

---

[6] Ordinary Differential Equation.

2.2. Recombination History

The problem of this work is to compute the optical depth, $\tau(x)$, and the so-called visibility function, $g(x)$, which is needed for integrating the Boltzmann-Einstein equations in future works, and computing the CMB power spectrum. Physical descriptions and derivations will not be given here, but can be found in the lecture notes above, in Callin (2006), or Dodelson (2003). Here only the required definitions will be presented.

Light that travels through a medium can be absorbed by the medium. If we have a source emitting an intensity I_0 then, an observer a distance x away from the source will observe an intensity $I(x) = I_0 e^{-\tau(x)}$. The quantity τ is called the optical depth. If $\tau \ll 1$ then the medium does nothing (we say its optically thin) and if $\tau \gg 1$ then we will see nothing (the medium is optically thick). The transition between these two regimes is when $\tau \sim 1$. In cosmology the main 'absorption' is Thompson scattering of photons of free electrons. The optical depth is defined as

$$
\tau(\eta) = \int_\eta^{\eta_0} n_e \sigma_T a d\eta', \tag{32}
$$

and quantifies the probability for scattering a photon between some previous time and today (the number of scatterings of photons by electrons per unit time is $c n_e \sigma_T$). The components involved in this expression are: $n_e = n_e(\eta)$; the electron density (the number of free electrons per cubic meter) at time η, $\sigma_T = \frac{8\pi}{3}\frac{\alpha^2\hbar^2}{m_e^2 c^2}$; the Thompson cross-section and the scale factor a. The transition between the Universe being optically thick and optically thin happens around recombination when most of the free electrons are captured by free protons to form neutral hydrogen. The expression for τ may also be written on an differential form, such that

$$
\tau' = \frac{d\tau}{dx} = -\frac{c n_e \sigma_T}{H}. \tag{33}
$$

This implies that existing routines can be used for solving differential equations to compute τ, if n_e can only be somehow compute at any time. And that's the difficult part. Instead of actually computing n_e, we rather focus on the fractional electron density, $X_e \equiv n_e/n_H$, where n_H is the proton density. If we will assume that all baryons are protons (no helium or heavier elements), then

$$
n_H = n_B \approx \frac{\rho_B}{m_H} = \frac{\Omega_{B,0}\rho_{c0}}{m_H a^3}, \tag{34}
$$

where $\rho_{c0} \equiv \frac{3H_0^2}{8\pi G}$ is the critical density of the universe today. If we do include Helium then only a (mass) fraction $1 - Y_p$ of the baryons are hydrogen so

$$
n_H = (1 - Y_p)n_B = (1 - Y_p)\frac{\Omega_{B,0}\rho_{c0}}{m_H a^3}, \tag{35}
$$

where m_H is the hydrogen mass and Y_p is the Helium fraction and is a new cosmological parameter (BBN[7] gives us $Y_p \approx 0.24$

---

[7] BigBang Nucleosynthesis

and observational constraints are consistent with this - the fiducial value in this work is $Y_p = 0$).

Now, there are two different equations available for X_e as a function of temperature and density, namely the so-called Saha and Peebles' equations (Equations 36 and 37 respectively). If we ignore Helium then the first one of these reads

$$\frac{X_e^2}{1 - X_e} = \frac{1}{n_B} \left(\frac{m_e T_B}{2\pi}\right)^{3/2} e^{-\epsilon_0/T_B}, \tag{36}$$

where T_B is the baryon temperature of the universe, and $\epsilon = 13.6$ eV is the ionization energy of hydrogen (the energy a photon needs in order to rip an electron away from a proton). In principle, one would have to solve separately for both T_B and the photon temperature, T_γ, but in practice it is an excellent approximation to set these equal. It can therefore be assumed that $T_B = T_\gamma = T_{CMB,0}/a$. With the above information, Equation 36 (Saha's equation) reduces to a standard second-order equation in X_e, and can be solved directly using the normal formula, $y = (-b \pm \sqrt{b^2 - 4ac})/2a$.

Saha's equation (Equation 36) is an excellent approximation when $X_e \approx 1$. When X_e is noticeably smaller than one, better approximations are required, and one such approximation is the Peebles' equation (Equation 37),

$$\frac{dX_e}{dx} = \frac{C_r(T_b)}{H} \left[\beta(T_b)(1 - X_e) - n_H \alpha^{(2)}(T_b) X_e^2\right], \tag{37}$$

where H is the Hubble parameter and

$$C_r(T_b) = \frac{\Lambda_{2s \to 1s} + \Lambda_\alpha}{\Lambda_{2s \to 1s} + \Lambda_\alpha + \beta^{(2)}(T_b)}, \quad \text{(dimensionless)}, \tag{38}$$

$$\Lambda_{2s \to 1s} = 8.227 s^{-1}, \quad \text{(dimension 1/s)}, \tag{39}$$

$$\Lambda_\alpha = H \frac{(3\epsilon_0)^3}{(8\pi)^2 n_{1s}}, \quad \text{(dimension 1/s)}, \tag{40}$$

$$n_{1s} = (1 - X_e) n_H, \quad \text{(dimension 1/m}^3\text{)}, \tag{41}$$

$$n_H = (1 - Y_p) \frac{3 H_0^2 \Omega_{b0}}{8\pi G m_H a^3}, \quad \text{(dimension 1/m}^3\text{)}, \tag{42}$$

$$\beta^{(2)}(T_b) = \beta(T_b) e^{3\epsilon_0/4T_b}, \quad \text{(dimension 1/s)}, \tag{43}$$

$$\beta(T_b) = \alpha^{(2)}(T_b) \left(\frac{m_e T_b}{2\pi}\right)^{3/2} e^{-\epsilon_0/T_b}, \quad \text{(dimension 1/s)}, \tag{44}$$

$$\alpha^{(2)}(T_b) = \frac{64\pi}{\sqrt{27\pi}} \frac{\alpha^2}{m_e^2} \sqrt{\frac{\epsilon_0}{T_b}} \phi_2(T_b), \quad \text{(dimension m}^3\text{/s)}, \tag{45}$$

$$\phi_2(T_b) = 0.448 \ln(\epsilon_0/T_b), \quad \text{(dimensionless)}, \tag{46}$$

where $\alpha \simeq \frac{1}{137.0359992}$ in the expression for $\alpha^{(2)}$ is the fine-structure constant. This looks a bit scary, but it's not too bad, really. First of all, the various constants are simply physical constants describing simple atomic physics; Peebles' equation takes into account the transition rates between the ground-state ($1s$) and the first excited state ($2s$) of the hydrogen atom. For even higher-accurate work, many more states should be included, and also other atoms, most notably the helium atom. But here the Peebles' equation is enough. Second, the Peebles' equation is simply yet another linear first-order differential equation.

Next, it is necessary to decide when to switch from Saha's equation to Peebles' equation. For simplicity, lets simply say that when $X_e > 0.99$, Saha's has to be used and when $X_e < 0.99$, Peebles' has to be used.

When n_e has been computed, the next step is to spline it, such that it can be evaluated at arbitrary values of x.

Now it is time to compute the optical depth, by solving Equation 33 mentioned above, with $\tau(x_{today}) = 0$ as the initial condition[8].

The final item to compute is the so-called visibility function,

$$\tilde{g}(x) = -\tau'(x) e^{-\tau(x)}, \tag{47}$$

which has the property that $\int_{-\infty}^0 \tilde{g}(x) dx = 1$. This function is therefore a true probability distribution, and describes the probability density for a given photon to last time having scattered at time x. As it will be seen, this function is sharply peaked around $x = -7$, corresponding to redshifts of $z \sim 1100$. The fact that this is so sharply peaked is the reason why we often refer to the recombination period as the surface of last scattering: This process happened during a very thin shell around us, at a redshift of $z \sim 1100$. The first and second order derivatives of $\tilde{g}$ will be also required, and so these must also be properly splined, just as τ was.

The final thing to compute is the so-called sound-horizon at decoupling (the total distance a sound-wave in the photon-baryon plasma can propagate from the Big Bang and until photons decouple). This quantity is not so relevant at the moment, but it will be important later in this project, since this length scale is imprinted in the CMB and the distribution of dark matter and galaxies in our Universe, so it is important to know how big it is. The sound-speed of the coupled photon-baryon plasma is slightly lower than the sound-speed of photons ($c/\sqrt{3}$) and

---

[8] Remember that the optical depth at our place in the universe today is precisely zero.

given by $c_s = c \sqrt{\frac{R}{3(1+R)}}$, where $R = \frac{4\Omega_{\gamma,0}}{3\Omega_{\mathrm{B},0}a}$, so the sound-horizon is

$$\frac{ds(x)}{dx} = \frac{c_s}{\mathcal{H}} \quad \text{with} \quad s(x_{\mathrm{ini}}) = \frac{c_s(x_{\mathrm{ini}})}{\mathcal{H}(x_{\mathrm{ini}})}. \tag{48}$$

Evaluating it at $x = x_{\mathrm{decoupling}}$ gives us the sound-horizon at decoupling $r_s \equiv s(x_{\mathrm{decoupling}})$.

2.3. Perturbations

During the lectures[9], the linearized Einstein and Boltzmann equations for photons, baryons and dark matter, and their respective inflationary initial conditions have been derived. One of the goals of the current study is to solve these equations numerically.

But before writing down the equations, there are a few issues that should be pointed out. First, at early times the optical depth, τ, is very large. The ODE we have to solve for the perturbations becomes numerically unstable in this regime and this must be dealt with. Large τ means that electrons at a given place only observe temperature fluctuations that are very nearby. This, in turn, implies that it will only see very smooth fluctuations, since the full system is in thermodynamic equilibrium, and all gradients are efficiently washed out. The only relevant quantities in this regime are therefore

1. The monopole, Θ_0, which measures the mean temperature at the position of the electron.
2. The dipole, Θ_1, which is given by the velocity of the fluid due to the Doppler effect.
3. The quadrupole, Θ_2, which is the only relevant source of polarization signals.

The regime where this is the case is called *tight coupling*.

At later times, though, the fluid becomes thinner, and the electrons start seeing further away, and then become sensitive to higher-ordered multipoles, Θ_l. Fortunately, because of a very nice computational trick due to Zaldarriaga and Seljak called *line of sight integration* [Seljak & Zaldarriaga (1996)], only a relatively small number of these (six is enough) needs to be taken into account, and so the system of relevant equations is therefore still tractable[10].

A second issue is the very large value of τ' at early times, which multiplies $(3\Theta_1 + v_B)$ in the Boltzmann equations. The latter factor is very small early on, and the product of the two is therefore numerically extremely unstable. The result is that the standard Boltzmann equation set is completely unstable if one simply implements the full expressions at early times. The solution to this problem is to use a proper approximation for $(3\Theta_1 + v_B)$ at early times. See the appendix for a derivation.

2.3.1. The full system

Photon temperature multipoles:

$$\Theta'_0 = -\frac{ck}{\mathcal{H}}\Theta_1 - \Phi', \tag{49}$$

$$\Theta'_1 = \frac{ck}{3\mathcal{H}}\Theta_0 - \frac{2ck}{3\mathcal{H}}\Theta_2 + \frac{ck}{3\mathcal{H}}\Psi + \tau'\left[\Theta_1 + \frac{1}{3}v_b\right], \tag{50}$$

$$\Theta'_\ell = \frac{\ell ck}{(2\ell+1)\mathcal{H}}\Theta_{\ell-1} - \frac{(\ell+1)ck}{(2\ell+1)\mathcal{H}}\Theta_{\ell+1} + \tau'\left[\Theta_\ell - \frac{\Pi\delta_{\ell,2}}{10}\right], \tag{51}$$

where $2 \leq \ell < \ell_{\mathrm{max}}$, and

$$\Theta'_{\ell_{\mathrm{max}}} = \frac{ck}{\mathcal{H}}\Theta_{\ell_{\mathrm{max}}-1} - c\frac{\ell_{\mathrm{max}}+1}{\mathcal{H}\eta(x)}\Theta_{\ell_{\mathrm{max}}} + \tau'\Theta_{\ell_{\mathrm{max}}}. \tag{52}$$

Photon polarization multipoles:

$$\Theta_0^{P'} = -\frac{ck}{\mathcal{H}}\Theta_{P1} + \tau'\left[\Theta_{P0} - \frac{1}{2}\Pi\right] \tag{53}$$

$$\Theta_\ell^{P'} = \frac{\ell ck}{(2\ell+1)\mathcal{H}}\Theta_{\ell-1}^P - \frac{(\ell+1)ck}{(2\ell+1)\mathcal{H}}\Theta_{\ell+1}^P + \tau'\left[\Theta_\ell^P - \frac{\Pi\delta_{\ell,2}}{10}\right], \tag{54}$$

where $1 \leq \ell < \ell_{\mathrm{max}}$, and

$$\Theta_{\ell_{\mathrm{max}}}^{P}{}' = \frac{ck}{\mathcal{H}}\Theta_{\ell_{\mathrm{max}}-1}^P - c\frac{\ell_{\mathrm{max}}+1}{\mathcal{H}\eta(x)}\Theta_{\ell_{\mathrm{max}}}^P + \tau'\Theta_{\ell_{\mathrm{max}}}^P. \tag{55}$$

Neutrino multipoles:

$$\mathcal{N}'_0 = -\frac{ck}{\mathcal{H}}\mathcal{N}_1 - \Phi', \tag{56}$$

$$\mathcal{N}'_1 = \frac{ck}{3\mathcal{H}}\mathcal{N}_0 - \frac{2ck}{3\mathcal{H}}\mathcal{N}_2 + \frac{ck}{3\mathcal{H}}\Psi \tag{57}$$

$$\mathcal{N}'_\ell = \frac{\ell ck}{(2\ell+1)\mathcal{H}}\mathcal{N}_{\ell-1} - \frac{(\ell+1)ck}{(2\ell+1)\mathcal{H}}\mathcal{N}_{\ell+1}, \tag{58}$$

where $2 \leq \ell < \ell_{\mathrm{max},\nu}$, and

$$\mathcal{N}'_{\ell_{\mathrm{max},\nu}} = \frac{ck}{\mathcal{H}}\mathcal{N}_{\ell_{\mathrm{max},\nu}-1} - c\frac{\ell_{\mathrm{max},\nu}+1}{\mathcal{H}\eta(x)}\mathcal{N}_{\ell_{\mathrm{max},\nu}}. \tag{59}$$

Cold dark matter and baryons:

$$\delta'_{\text{CDM}} = \frac{ck}{\mathcal{H}} v_{\text{CDM}} - 3\Phi', \tag{60}$$

$$v'_{\text{CDM}} = -v_{\text{CDM}} - \frac{ck}{\mathcal{H}}\Psi, \tag{61}$$

$$\delta'_B = \frac{ck}{\mathcal{H}} v_B - 3\Phi', \tag{62}$$

$$v'_B = -v_B - \frac{ck}{\mathcal{H}}\Psi + \tau' R(3\Theta_1 + v_B). \tag{63}$$

Metric perturbations:

$$\Phi' = \frac{H_0^2}{2\mathcal{H}^2}\left[\frac{\Omega_{\text{CDM0}}}{a}\delta_{\text{CDM}} + \frac{\Omega_{B0}}{a}\delta_B + 4\frac{\Omega_{\gamma 0}}{a^2}\Theta_0 + 4\frac{\Omega_{\nu 0}}{a^2}\mathcal{N}_0\right]$$
$$+ \Psi - \frac{c^2 k^2}{3\mathcal{H}^2}\Phi, \tag{64}$$

$$\Psi = -\Phi - \frac{12H_0^2}{c^2 k^2 a^2}\left[\Omega_{\gamma 0}\Theta_2 + \Omega_{\nu 0}\mathcal{N}_2\right]. \tag{65}$$

In the equations above $\Pi = \Theta_2 + \Theta_0^P + \Theta_2^P$ and $R = \frac{4\Omega_{\gamma 0}}{3\Omega_{B0}a}$.

2.3.2. The tight coupling regime

Just solving the original ODE system for all times would be ideal, however this does not work as the system is very stiff and numerically unstable when τ is very large. Some slightly different equations in the tight coupling regime therefore have to be solve . In the tight coupling regime, the only differences are:

1. That one should only include $\ell = 0$ and 1 for Θ_ℓ and none for polarization (all higher moments are given by those).
2. That the expressions for Θ'_1 and v'_B are quite a bit more involved:

$$\text{Num.} = \left[(1-R)\tau' + (1+R)\tau''\right](3\Theta_1 + v_B) - \frac{ck}{\mathcal{H}}\Psi +$$
$$\left(1 - \frac{\mathcal{H}'}{\mathcal{H}}\right)\frac{ck}{\mathcal{H}}(-\Theta_0 + 2\Theta_2) - \frac{ck}{\mathcal{H}}\Theta'_0 \tag{66}$$

$$\text{Den.} = (1+R)\tau' + \frac{\mathcal{H}'}{\mathcal{H}} - 1 \tag{67}$$

$$q = -\frac{\text{Num.}}{\text{Den.}}, \tag{68}$$

$$v'_B = \frac{1}{1+R}\left[-v_B - \frac{ck}{\mathcal{H}}\Psi + R\left(q + \frac{ck}{\mathcal{H}}(-\Theta_0 + 2\Theta_2) - \frac{ck}{\mathcal{H}}\Psi\right)\right] \tag{69}$$

$$\Theta'_1 = \frac{1}{3}(q - v'_B) \tag{70}$$

In the tight coupling regime, we get the same expressions for the higher-ordered photon moments as given by the initial conditions,

$$\Theta_2 = \begin{cases} -\frac{8ck}{15\mathcal{H}\tau'}\Theta_1, & \text{(with polarization)} \\ -\frac{20ck}{45\mathcal{H}\tau'}\Theta_1, & \text{(without polarization)} \end{cases} \tag{71}$$

$$\Theta_\ell = -\frac{\ell}{2\ell+1}\frac{ck}{\mathcal{H}\tau'}\Theta_{\ell-1}, \qquad \ell > 2, \tag{72}$$

$$\Theta_0^P = \frac{5}{4}\Theta_2, \tag{73}$$

$$\Theta_1^P = -\frac{ck}{4\mathcal{H}\tau'}\Theta_2, \tag{74}$$

$$\Theta_2^P = \frac{1}{4}\Theta_2, \tag{75}$$

$$\Theta_\ell^P = -\frac{\ell}{2\ell+1}\frac{ck}{\mathcal{H}\tau'}\Theta_{\ell-1}^P, \qquad \ell > 2. \tag{76}$$

2.3.3. Initial conditions

The initial conditions are given by:

$$\Psi = -\frac{1}{\frac{3}{2} + \frac{2f_\nu}{5}}, \tag{77}$$

where $f_\nu = \frac{\Omega_{\nu 0}}{\Omega_{\gamma 0} + \Omega_{\nu 0}}$,

$$\Phi = -(1 + \frac{2f_\nu}{5})\Psi, \tag{78}$$

$$\delta_{\text{CDM}} = \delta_B = -\frac{3}{2}\Psi, \tag{79}$$

$$v_{\text{CDM}} = v_B = -\frac{ck}{2\mathcal{H}}\Psi, \tag{80}$$

Photons:

$$\Theta_0 = -\frac{1}{2}\Psi, \tag{81}$$

$$\Theta_1 = \frac{ck}{6\mathcal{H}}\Psi, \tag{82}$$

$$\Theta_2 = \begin{cases} -\frac{8ck}{15\mathcal{H}\tau'}\Theta_1, & \text{(with polarization)} \\ -\frac{20ck}{45\mathcal{H}\tau'}\Theta_1, & \text{(without polarization)} \end{cases} \tag{83}$$

$$\Theta_\ell = -\frac{\ell}{2\ell+1}\frac{ck}{\mathcal{H}\tau'}\Theta_{\ell-1}, \tag{84}$$

Photon polarization:

$$\Theta_0^P = \frac{5}{4}\Theta_2, \tag{85}$$

$$\Theta_1^P = -\frac{ck}{4\mathcal{H}\tau'}\Theta_2, \tag{86}$$

$$\Theta_2^P = \frac{1}{4}\Theta_2, \tag{87}$$

$$\Theta_\ell^P = -\frac{\ell}{2\ell+1}\frac{ck}{\mathcal{H}\tau'}\Theta_{\ell-1}^P, \tag{88}$$

Neutrinos:

$$\mathcal{N}_0 = -\frac{1}{2}\Psi, \tag{89}$$

$$\mathcal{N}_1 = \frac{ck}{6\mathcal{H}}\Psi, \tag{90}$$

$$\mathcal{N}_2 = -\frac{c^2 k^2 a^2 (\Phi + \Psi)}{12 H_0^2 \Omega_{\nu 0}}, \tag{91}$$

$$\mathcal{N}_\ell = \frac{ck}{(2\ell+1)\mathcal{H}}\mathcal{N}_{\ell-1}, \qquad \ell \geq 3. \tag{92}$$

Note that Ψ is not a dynamical variable in the code and is only used here to set the rest of the variables. Since the equation system is linear, (we are free to choose) the normalization of Ψ can be freely chosen when we solving it (the normalization has be done in the end). The particular normalization used here is such that when computing the power-spectra then $\Psi_{\text{true}}^2 = \Psi_{\text{code}}^2 \mathcal{P}_\mathcal{R}$ where $\mathcal{P}_\mathcal{R}$ is the usual curvature perturbation power-spectrum, the perturbations set up by inflation, $\mathcal{P}_\mathcal{R}(k) = A_s (k/k_{\text{pivot}})^{n_s - 1}$ with $A_s, n_s, k_{\text{pivot}}$ (primordial amplitude, spectral index and the pivot scale) being the same parameters as is standard in the literature (and used in codes like CAMB and CLASS).

2.4. CMB power-spectrum

Knowing the ionization history of the universe and knowing how structure have grown from the very earliest epochs, the CMB power-spectrum can be computed now. Pulling it all together is what has to be done in order to derive our preferred observable, namely the CMB power spectrum.

In order to understand how to get to the CMB power spectrum from our computed quantities, let us first recall the definition of the spherical harmonics transform of the CMB temperature field,

$$T(\hat{n}) = \sum_{\ell m} a_{\ell m} Y_{\ell m}(\hat{n}), \tag{93}$$

where $\hat{n}$ is the direction on the sky, $a_{\ell m}$ are the spherical harmonics coefficients, and $Y_{\ell m}$ are the spherical harmonics themselves.

The CMB power spectrum, on the other hand, is simply defined as the expectation value of the square of the spherical harmonics coefficients[11],

$$C_\ell \equiv \left\langle |a_{\ell m}|^2 \right\rangle = \left\langle a_{\ell m} a_{\ell m}^* \right\rangle. \tag{94}$$

So, in order to get to the power spectrum, the temperature field we observe around us today $T(\hat{n}, x = 0)$ has to be known. But fortunately, we already have this information is (more or less) available, since the evolution of the temperature field, in the form of $\Theta_\ell(k, x)$, has already been computed. The values of these functions at $x = 0$ have been read off, the resulting coefficients (to get $T(\boldsymbol{n})$ instead of $T(\boldsymbol{k})$) have been Fourier transformed, and the correct values have been read off.

---

[11] Note that, in principle, this function should have two subscripts, $C_{\ell m}$, but because we assume that the universe is isotropic, it must have the same power spectrum towards both the x, y and z directions, and this implies full rotational invariance. As a result, there is no m dependence in the power spectrum, and we simply average over m, and only call the spectrum C_ℓ.

But these functions have only been computed up to $\ell = 6$, and smaller scales than that are surely interesting! Knowing the power spectrum to at least $\ell = 1200$ is what is required in order to compute the CMB power-spectrum. So the code has been rerun, but this time with $\ell_{max} = 1200$ instead of 6. The only problem with that is that it will take a ***very*** long time to complete.

This is where the method of Zaldarriaga and Seljak comes to our rescue, through what they call the line-of-sight integration approach [Seljak & Zaldarriaga (1996)]. What we really need to know, is $\Theta(k, \mu, x = 0)$. But instead of first expanding the full temperature field in multipoles and then solve the coupled equations, one can start by formally integrating the original equation for $\dot{\Theta}$, and then expand in multipoles at the end. For the details of this process, as in Callin (2006) or **?**. The final expression is simply

$$\Theta_\ell(k, x = 0) = \int_{-\infty}^{0} \tilde{S}(k, x) j_\ell[k(\eta_0 - \eta)]dx, \qquad (95)$$

where the ***source function*** is defined as

$$\tilde{S}(k, x) = \tilde{g}\left[\Theta_0 + \Psi + \frac{1}{4}\Pi\right] + e^{-\tau}[\Psi' - \Phi'] - \frac{1}{ck}\frac{d}{dx}(\mathcal{H}\tilde{g}v_b)$$

$$+ \frac{3}{4c^2k^2}\frac{d}{dx}\left[\mathcal{H}\frac{d}{dx}(\mathcal{H}\tilde{g}\Pi)\right], \qquad (96)$$

where all quantities have been computed in earlier works.

The intuition behind this approach is that the observed CMB radiation in a given direction on the sky, is basically the integral of the local CMB monopole (weighted by the visibility function) along the line of sight from us to infinity. That's the first Θ_0 term in the source function. However, there are a number of corrections to this effect. First, the Ψ term encodes the fact that the photons have to climb out of a gravitational potential, and therefore loose energy on its way to us. Π is a small quadrupolar (plus polarization if it has been included) correction to the original monopole contribution.

The next main term is essentially the so-called Integrated Sachs-Wolfe contribution, which describes the fact that gravitational potentials actually change while the photons are moving. The third term is a Doppler term and the fourth term is a consequence of the angular dependence of Thompson scattering (photons are more likely to be scattered in certain directions than others).

So, this is a much more beautiful approach: Instead of evaluating what every single photon moment is at our position today, the monopole can be computed at all positions and times, and then the integral is done through space. Much faster, and also quite intuitive.

The $j_\ell(x)$'s in the above expression are the so-called spherical Bessel functions, and take into account the projection of the 3D field (characterized by k) onto a 2D sphere (characterized by ℓ).

Now, how to compute $\Theta_\ell(k)$ is known, however going to actual C_ℓ's is still needed. This corresponds to

1. Taking the square of $\Theta_\ell(k)$ (since C_ℓ is the square of the Fourier coefficients).
2. Multiplying with the primordial power spectrum $P_{primordial}(k)$ coming from inflation (recall that Φ was originally set $\Phi \sim 1$ for all modes; this is now corrected by rescaling everything by $P(k)$ instead, which is perfectly valid, since all the used equations are linear).
3. Integrating over all three spatial directions, instead of just the z direction (but since isotropy is assumed, the same derived functions for all three directions can be used).

The CMB power spectrum then reads

$$C_\ell = \frac{2}{\pi}\int k^2 P_{primordial}(k)\Theta_\ell^2(k)dk. \qquad (97)$$

However, this can be massaged a bit further, by noting that most inflation models predict a so-called Harrison-Zel'dovich spectrum, for which

$$\frac{k^3}{2\pi^2}P_{primordial}(k) = A_s\left(\frac{k}{k_{pivot}}\right)^{n_s-1}, \qquad (98)$$

where n_s is the spectral index of scalar perturbations ($n_s \sim 0.96$), and expected to be close to unity, k_{pivot} is some scale for which the amplitude is A_s (for $k_{pivot} = 0.05/\text{Mpc}$ we have $A_s \sim 2 \cdot 10^{-9}$ for our Universe). The final expression for the spectrum is therefore

$$C_\ell = 4\pi\int_0^\infty A_s\left(\frac{k}{k_{pivot}}\right)^{n_s-1}\Theta_\ell^2(k)\frac{dk}{k}. \qquad (99)$$

Two final comments: First, the power spectrum is most often plotted in units of $\ell(\ell+1)/2\pi$ in μK^2, because it's overall trend is to drop as ℓ^{-2}. It is therefore easier to see features when plotted in these units (i.e. you multiply C_ℓ by $\frac{\ell(\ell+1)}{2\pi}\left(10^6 T_{CMB0}\right)^2$).

The matter power-spectrum has also been computed. This is really easy, only multiplying some numbers together is needed:

$$P(k, x) = |\Delta_M(k, x)|^2 P_{primordial}(k), \qquad (100)$$

where $\Delta_M(k, x) \equiv \frac{c^2 k^2 \Phi(k,x)}{\frac{3}{2}\Omega_{M0}a^{-1}H_0^2}$ and $\Omega_{M,0}$ is the total matter density parameter today. It has only been computed for $x = 0$, i.e. today. This is often plotted as k in units of h/Mpc versus $P(k)$ in units of $(\text{Mpc}/h)^3$. To explain this plot it has been useful to mark in the equality scale $k_{eq} = \frac{a_{eq}H(a_{eq})}{c}$ in the plot where a_{eq} is the scale-factor for matter-radiation equality.

2.4.1. Generate a CMB map

From the theoretical C_ℓ spectrum a CMB map can be generated. Generating a map is a fairly straight forward thing to do, but the hard part of this is to pixelate the sphere and project that down to a 2D map that we can plot. Luckily there is a great library for this namely the HEALPIX library[12] (for this you also need

---

[12] https://healpix.sourceforge.io/downloads.php

the CFITSIO library[13]). There is also a Python wrapper for this library called Healpy[14]. This library can be supplied with the C_ℓ's or a realization of the $a_{\ell m}$'s (which can be generated from the C_ℓ's) and have it provide the map.

Healpix has routines for generating maps directly from a power-spectrum or from $a_{\ell m}$'s. If you want to generate your own realization of $T(\hat{n})$ then note that the $a_{\ell m} = x + iy$ with x, y being random numbers drawn from a Gaussian distribution with variance $C_\ell/\sqrt{2}$. A simple way to generate a realization is to draw (for each value of ℓ, m) two random numbers A, θ from a uniform distribution on $[0, 1)$ and set

$$a_{\ell m} = \sqrt{-\log(A)C_\ell}e^{2\pi i\theta}. \tag{101}$$

Note that $T = T^*$ is real, so

$$a_{\ell,-m} = (-1)^m a_{\ell m}^*, \tag{102}$$

and we only need to generate them for $m \geq 0$. The other way around: if you want to estimate the angular power-spectrum from a set of $a_{\ell m}$'s by computing

$$\hat{C}_\ell = \frac{1}{2\ell + 1} \sum_{m=-\ell}^{\ell} |a_{\ell m}|^2. \tag{103}$$

This should give you back the input power-spectrum for large ℓ (and will suffer from cosmic variance for small ℓ).

3. Implementation method

3.1. BackgroundCosmology

A class that takes in all the cosmological parameters (h, $\Omega_{\text{B},0}$, $\Omega_{\text{CDM},0}$, $\Omega_{k,0}$, $T_{\text{CMB},0}$, N_{eff}), computes $\Omega_{\gamma,0}$, $\Omega_{\nu,0}$ and $\Omega_{\Lambda,0}$ from these and stores them has been implemented in a C++ code[15]. Functions that are able to get the cosmological parameters, the Hubble function and $\mathcal{H} = aH$ ("Hp") plus the first two derivatives (these have been computed analytically) together with the different distance measures (co-moving, luminosity and angular diameter distance) have been made. Once this was done, $\eta(x)$ was computed, spline the result was splined and a function that returns this function was made [Callin (2006)].

Then, equality times and acceleration time plus the age of the Universe were computed. This was done in the same way as for the conformal time by solving an ODE and making a spline of $t(x)$ (useful for computing the time at any x later on if needed). Evaluating the spline at $x = 0$ gives the time of the Universe in seconds (if using SI units), but it was converted to a more sensible unit, like gigayears ($109 \cdot 365 \cdot 24 \cdot 60 \cdot 60$ seconds), when presenting the results.

Once the distance measures were working, the parameter fits to supernova data [Betoule et al. (2014)] was made. First the results of the luminosity distance were plotted, using the fiducial cosmological parameters from Section 1, together with the data points from supernova observations. The fitting routine is a simple Metropolis Monte Carlo Markov Chain (MCMC) sampler. After everything has been implemented, the code was used to get constraints on our cosmological parameters by comparing to data.

The used data was a set of supernova with associated redshift z_i, luminosity distance $d_L^{\text{obs}}(z_i)$ and associated measurement errors σ_i. Under the assumption that the measurements are Gaussian distributed and uncorrelated between different redshifts, the Likelihood function (telling how well the data fit the theory), is given by $\mathcal{L} \propto e^{-\chi^2/2}$ where the chi-squared function is

$$\chi^2(h, \Omega_{\text{M},0}, \Omega_{k,0}) = \sum_{i=1}^{N} \frac{\left[d_L(z_i, h, \Omega_{\text{M},0}, \Omega_{k,0}) - d_L^{\text{obs}}(z_i)\right]^2}{\sigma_i^2}. \tag{104}$$

A low value of χ^2 means a good fit (high likelihood for the choice of parameters). The goal is to basically check all possible values of the parameters to find the best-fitting model and the range of parameters around it which are in agreement with the observed values. One can do this brute-force, but this step is in practice most commonly done by performing a so-called MCMC to randomly sample from the likelihood. The result from performing this step is a chain of values: parameter-points and likelihood values. The set of parameters with the lowest likelihood is the best-fit model. It can be checked if this is really a good fit by comparing the χ^2 to the number of data-points (here $N = 31$). A good fit has $\chi^2/N \sim 1$ (a much higher value denotes a bad fit). When the best-fit has been found, 1σ (68.4%) confidence region can be found by looking at all values that satisfies $\chi^2 - \chi^2_{\text{min}} < 3.53$. It is exactly the same for the 2σ (95.45%) confidence region by looking at all values that satisfies $\chi^2 - \chi^2_{\text{min}} < 8.04$[16].

3.2. RecombinationHistory

A class that takes in recombination parameters and a BackgroundCosmology object, has been implemented in a C++ code[17]. This has been used to solve the recombination history of the Universe.

The code starts by solving for the electron density n_e (X_e) by solving the Saha and Peebles equations (Equations 36 and 37 respectively). The former is easy: it's just a quadratic equation for X_e so it is easy to solve. However, the analytical solution at early times will be on the form "huge" ("huge" which should give approximately 1) so it has been needed to use the approximation $\sqrt{1 + x} \approx 1 + \frac{x}{2}$ when $|x| \ll 1$. The Saha equation is only valid as long as $X_e \approx 1$ so the code switches to the Peebles equation when $X_e < 0.99$. The result has been splined for X_e and n_e as this was needed when computing τ.

---

[13] https://heasarc.gsfc.nasa.gov/fitsio/
[14] https://healpy.readthedocs.io/en/latest/
[15] All the used code is fully available in my public GitHub repository.

[16] Robert Reid, Chi-squared distribution table with sigma values: http://www.reid.ai/2012/09/chi-squared-distribution-table-with.html
[17] All the used code is fully available in my public GitHub repository.

Once n_e has been computed[18], the ODE for τ (Equation 33) has been integrated from $x = 0$ and going back in time. The integration constant has been fixed by ensuring $\tau(x = 0) = 0$.

3.3. Perturbations

A class that takes in a BackgroundCosmology and RecombinationHistory object and uses this to evolve the perturbations of the Universe, has been implemented in a C++ code[19].

However one thing that complicates it is that when integrating the perturbations the full system cannot just be integrated directly (it is unstable due to the tight coupling between photons and baryons in the very early Universe). It was therefore needed to start off solving the tight coupling system: here only two photon multipoles Θ_0 and Θ_1 (and no polarization multipoles) had to be included. Once tight coupling ends, it was needed to switch to the full system. When doing this the initial conditions will be settled from the tight coupling solution plus giving a value to the multipoles present in the full system, but the tight-coupling regime (the value of these are given by the same relations as in the initial conditions, e.g. Θ_2 is given by the value of Θ_1) is not included. This means two functions were made to set initial conditions to the ODE vector (one at the start and one after tight coupling end) and two functions that sets the right hand side of the ODE system (one for tight coupling and one for the full system) have been implemented. Once this had been done, a vector of k-values was made, for which the system was solved and the perturbations were integrated from the start until today for all these k-values. The results of the ODE were extracted, stored and splined for all of the quantities (δ_B, v_B, Φ, Θ_0, etc.) that are required in the line-of-sight integrals.

The vector of the perturbations that we integrate will have between 10 and 30 or so elements depending on how many multipoles are included (and this vector will be different in the two regimes). This means it is very important to keep track over which index in the vector corresponds to which quantity.

3.4. PowerSpectrum

A class that takes in a BackgroundCosmology RecombinationHistory and a Perturbations object and uses this to compute $\Theta_\ell(k, x = 0)$ for $2 < \ell < 1200$ using line-of-sight integration and integrate this again to obtain the power-spectrum has been implemented in a C++ code[20].

The Perturbations class has been modified, adding a few more lines of code to make sure of the computations and storage of the source-function defined above. This is what needed in order to do the line-of-sight integration. Bessel-functions have also been needed.[21]

There are several ways you can do the line of sight integration:

---

1. Just evaluate the integral directly as in Callin (2006).
2. Evaluate the integral by treating it as an ODE and using the ODE solver (be careful with the accuracy settings of the ODE solver), i.e.

$$\frac{d\Theta_\ell(k, x)}{dx} = \tilde{S}(k, x) j_\ell[k(\eta_0 - \eta)], \quad \Theta_\ell(k, -\infty) = 0 \quad (105)$$

Same goes for the integration of the C_ℓ's.

4. Results

4.1. Solving the background cosmology of the Universe

The evolution of the relative energy densities of the Universe is presented in Figure 1. Here, each component is plotted, together with the combined contribution from all non-relativistic (baryonic/ordinary and cold dark) matter and all the relativistic particles (photons and neutrinos). It can clearly be seen that there are three different regimes, where each component (relativistic particles/radiation, marked with orange, non-relativistic matter, marked with blue, and dark energy/Λ, marked with green). This color coding has been used to better visualize these regimes in all the produced plots.
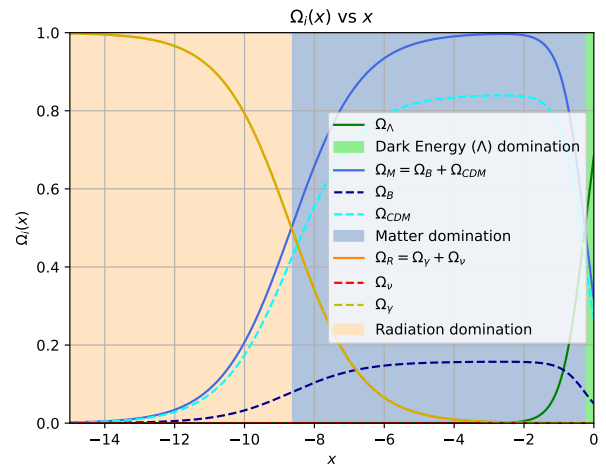

Fig. 1. Plot showing relative density parameters against the natural logarithm of the scale factor ($x = \ln a$). The early Universe was dominated by radiation, marked in orange. Following is the matter dominated era is marked in blue, where the combined density of the dark matter and baryon components is indicated by the blue line. Lastly, the present era is dominated by dark energy, marked in green.

From the splines created to solve the ODEs and compute both the cosmological time (Figure 2) and the conformal time (Figure 3) can be seen how they evolve in the different epoch of domination. From this data, one can compute both the age of the Universe and the conformal time today, being these $t_{\text{Universe}} = t(\text{today}) = t(0) \approx 13.86$ Gyr and $\eta(0)/c \approx 46.52$ Gyr, respectively. It also possible to compute the times when there was a radiation-matter and matter-dark energy equalities, along with the time at which the Universe started to accelerate, being this times summarized in Table 1.

As can be seen in Figure 2, cosmological time grows as the scale factor tends to 1 (if $a = e^x$ and $x \to 0 \Rightarrow a \to 1$). It can be inferred form the plot that cosmological time also grows

---

[18] Because n_e varies over many, many orders of magnitude, it is useful to spline $\ln(n_e)$ rather than n_e itself; this function varies much more slowly with x, and is therefore easier to interpolate.

[19] All the used code is fully available in my public GitHub repository.

[20] All the used code is fully available in my public GitHub repository.

[21] The ComplexBessel library should be installed, to do this check the GitHub page for how to do it). The fallback if you do not install it is to use the GSL, which is quite buggy for large ℓ.

	x	z	t [Gyr]
Radiation-matter	-8.67	5803.51	$2.28 \cdot 10^{-5}$
Matter-dark energy	-0.26	0.29	10.35
Accelerated expansion	-0.42	0.53	8.42

Table 1. Times at which there was radiation-matter equality, being this time expressed as the natural logarithm of the scale factor (x), redshift (z) and the cosmological time (t). The times of at which there was matter-dark energy equality and the time at which the Universe began its accelerated expansion are also shown.
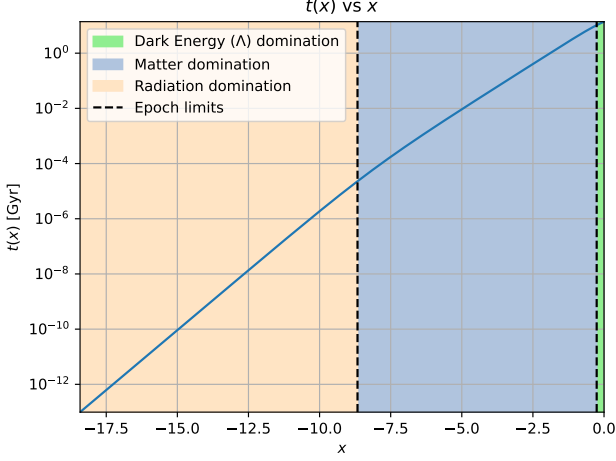
Fig. 2. Cosmological time evolution as a function of the natural logarithm of the scale factor.

exponentially, concluding that times is just another dimension (like the three spatial dimensions).
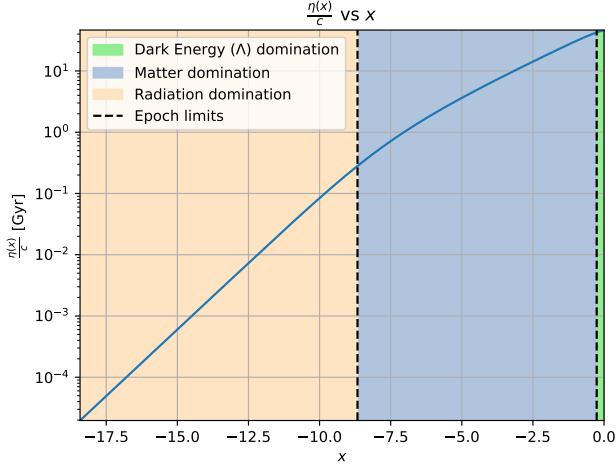
Fig. 3. Cosmological time evolution as a function of the natural logarithm of the scale factor.

The main result from this work is shown in Figure 4. Here are the conformal Hubble parameter (4a) is shown against x. It can be seen how this parameter decreases steeply in the radiation domination epoch, before getting into the matter domination epoch with a slightly gentler slope. The conformal time is, basically, the inverse of the conformal Hubble parameter. While the conformal Hubble parameter has an even steeper decrease in the radiation domination epoch going over to a less steep

decrease in the matter domination epoch.

Note that the Hubble prime starts to increase again when getting into the last regime, dominated by dark energy, which corresponds to an accelerated expansion like we observe today.

(a) Conformal Hubble parameter.   (b) Conformal time.
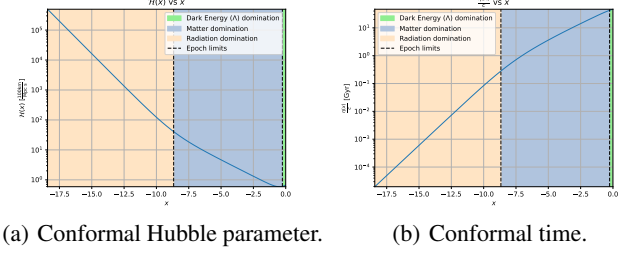
Fig. 4. Plots showing the evolution of the conformal Hubble parameter (4a) and the conformal time (4b).

Some ways of testing the code is studying the evolution of the (first, 5b, and second, 5a) derivatives of the conformal Hubble parameter with respect to x and the conformal Hubble parameter itself, as can be seen in Figure 5.
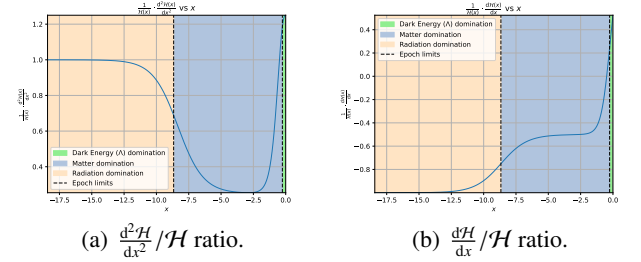

(a) $\frac{\mathrm{d}^2 \mathcal{H}}{\mathrm{d}x^2} / \mathcal{H}$ ratio.   (b) $\frac{\mathrm{d}\mathcal{H}}{\mathrm{d}x} / \mathcal{H}$ ratio.

Fig. 5. 5a: Ratio between the first derivative of $\mathcal{H}$ with respect to x and $\mathcal{H}$. 5b: Ratio between the first derivative of $\mathcal{H}$ with respect to x and $\mathcal{H}$.

Other check one can do is plotting the conformal time times the conformal Hubble parameter, which in the radiation domination epoch tends to 1. As can be seen from Figure 6, the further to the left, the closest to 1, so it can be assumed that when the curve is prolonged far enough it will asymptotically tend to 1.

Once it is clear that the code works (except for that mistake when computing the time at which the accelerated expansion of the Universe starts), the next step to check how good is the code is to try to get the parameters that fit better to some observations. For this, the data from Betoule et al. (2014) has been studied and fitted with a MCMC. The results of the fit are shown in Figure 7.

In Figure 8, the 1σ and 2σ deviation from the best fit parameters can be seen, showing in a dashed black line the set of parameters corresponding to a flat Universe. This deviations have been computed by choosing the parameters with a χ^2 greater by 3.53 (for the 1σ deviation) and by 8.04 (for the 2σ deviation) than the minimum value of χ^2 (the one of the best fitting parameters). A summary of values of the best fitting parameters can be found in Table 2.
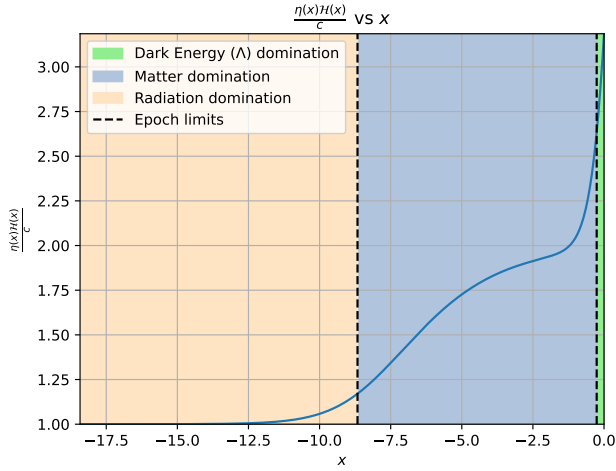
Fig. 6. Plot showing the relation between the conformal time and the conformal Hubble factor, showing that their product tends to 1 during the radiation domination epoch. It can also be seen that it is always of the order of 10^0.
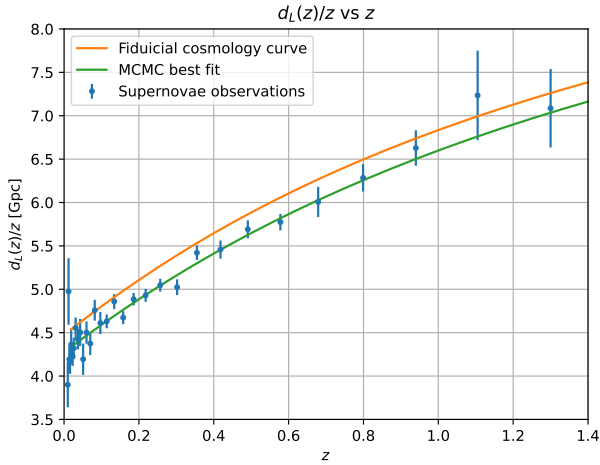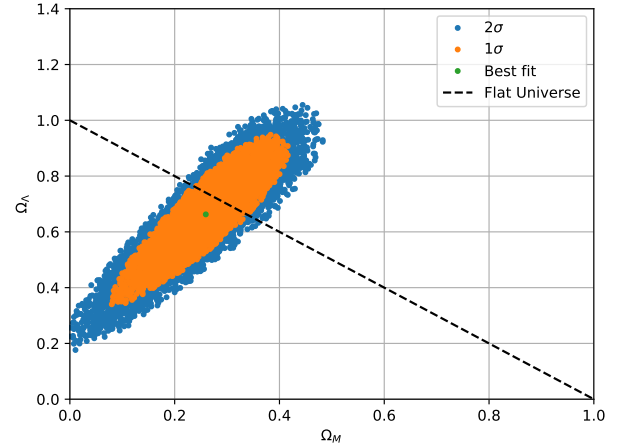

Fig. 8. Plot showing 1σ and 2σ deviation from the best fit parameters, showing in a dashed black line the set of parameters corresponding to a flat Universe.
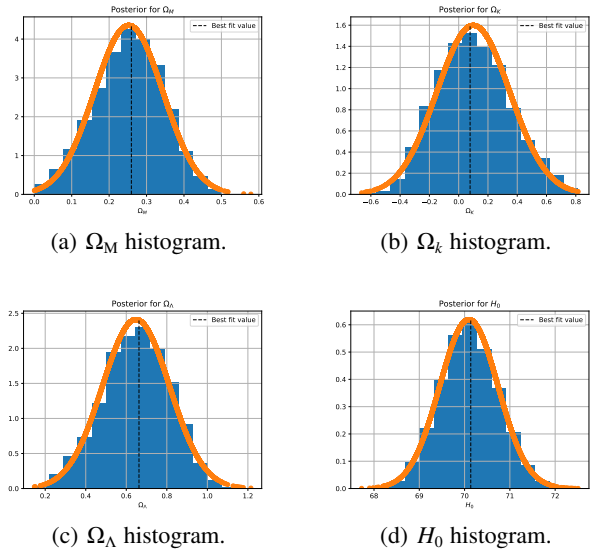

Fig. 7. Plot showing the observational data from Betoule et al. (2014) and the fit computed with the fiducial cosmology and with the MCMC fit, selecting the best parameters by choosing those corresponding to the lowest χ^2.

(a) Ω_M histogram.

(b) Ω_k histogram.

(c) Ω_Λ histogram.

(d) H_0 histogram.

Fig. 9. Histograms of the generated parameters: Ω_M (9a), Ω_k (9b), Ω_Λ (9c) and H_0 (9d) The best fitting parameters are shown in Table 2.

In Figure 9, a collection of histograms, showing the Gaussian distribution, of the generated parameters for the fitting parameters, along with a dashed black line showing the best fitting parameters.

χ^2	Ω_M	Ω_k	Ω_Λ	H_0
29.33	0.26	0.08	0.66	70.14

Table 2. Best fitting parameters from the supernova fitting via MCMC.

One could be surprised to see that some parameters are negative or greater than one, but if the sum of all the Ωs were to be computed, it will give a result of exactly 1. All Ωs should be greater or equal than 0 and smaller or equal to 1, except for $\Omega_k < 0$, which is perfectly a physical result since $\Omega_k \propto k$, and k can be negative if the Universe is openly curved (hyperbolic). From the histograms it can be expected to live in a Uni-

verse with around 26% matter, around 66% dark energy (Λ) and a flat (or slightly closely curved/spherical) Universe ($\Omega_k = 0.08$).

As can bee seen in Figure 9c, the fit of the data do not allow a negative cosmological constant, which implies that most of our Universe is unknown to us and further research is needed. Focusing now in Figure 9d, one can see that the best fitting parameter is slightly bigger than the fiducial H_0 ($H_0 = 67$ km/s/Mpc). This discrepancy is what is called the Hubble tension, whose cause is not known. This discrepancy arises when comparing the computed H_0 with "early" and "late" Universe observations.

4.2. Solving the recombination history of the Universe

First of all, the different times for decoupling, last scattering, half-way recombination (using only Saha's equation and using both Saha's and Peebles') and the recombination time have been

computed, being these times summarized in Table 3.

	x	z	t [Myr]
Decoupling	-7.370	1586.94	0.218
Last scattering	-6.987	1081.31	0.409
Half-way rec.	-7.164	1290.67	0.306
Half-way rec (Saha)	-7.230	1379.48	0.275
Recombination	-6.989	1083.10	0.408

Table 3. Summary of all the computed times in both redshift (z) and cosmological time (t).

The evolution of the free electron fraction is shown in Figure 10. Here it can be seen how the free electron fraction stay constant at 1 in the early Universe, before recombination happens. Then, at $x = x_{\text{recombination}} \approx -6.989$ we enter the Peebles' regime, and shortly after it can be seen that the free electron fraction start to evolve quite rapidly. At this point, the temperature of the Universe has dropped significantly, so free electrons and protons can start to form atoms of neutral hydrogen. As can be inferred from Table 3, at $x = -7.164$ we are half way through recombination (using the complete solution)[22]. Equation 36 has a exponential drop, which can be recognized in Figure 10, the $X_{e,\text{Saha}}$ solution drops off to zero with decreasing temperature. The full solution does not fall off exponentially, and instead flattens out to a stable value. This flattening can be described by two phases. First the free electrons decouple from the rest of the Universe as their interaction rate with the free protons drops below the expansion rate of the Universe. Second the free electrons freeze out, where the free electron fraction stops evolving and becomes, approximately, constant.
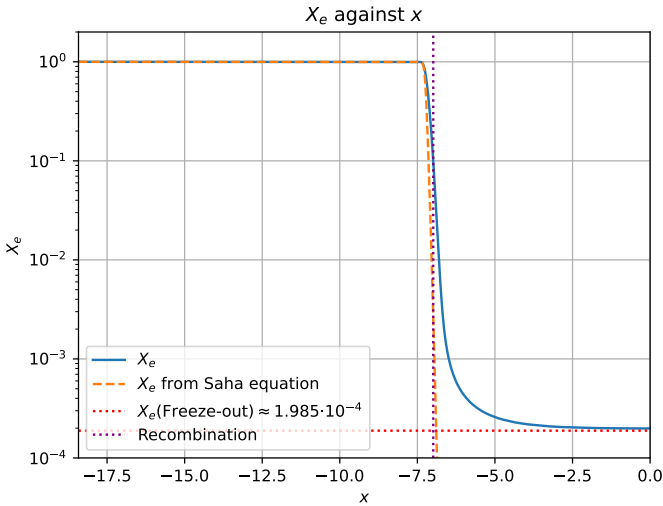
depth, and high free electron fraction. Where $\tau \gg 1$, the Universe was opaque. During radiation domination era, Universe expands proportionally to $\sqrt{t}$, so the optical "thickness" of the Universe is only decreasing along with the expansion. When recombination starts and X_e drops, it follows with a drop in the optical depth and its derivatives. This is consistent with less free electrons, so less Thompson scattering and longer mean free path. Now the optical "thickness" of the Universe has changed due to the change in the constituents of the Universe, not only the expansion.
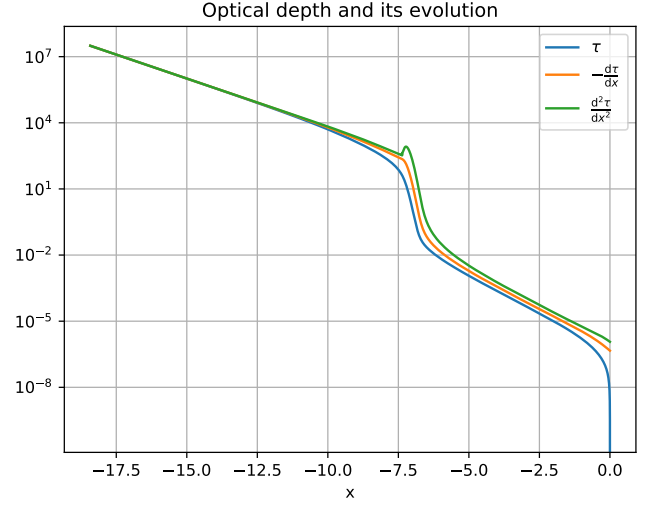

Fig. 11. Plot showing the optical depth (τ) and its two first derivatives.

Fig. 10. Plot showing the free electron fraction X_e. The solution obtained using only Saha's equation, which drops off exponentially to zero once the solution deviates from equilibrium, has been included.

In Figure 11, the optical depth and its derivatives have been plotted. In the dense primordial Universe, the mean free path of photons was really low due to Thompson's scattering on the abundant free electrons. This can be seen in the high optical
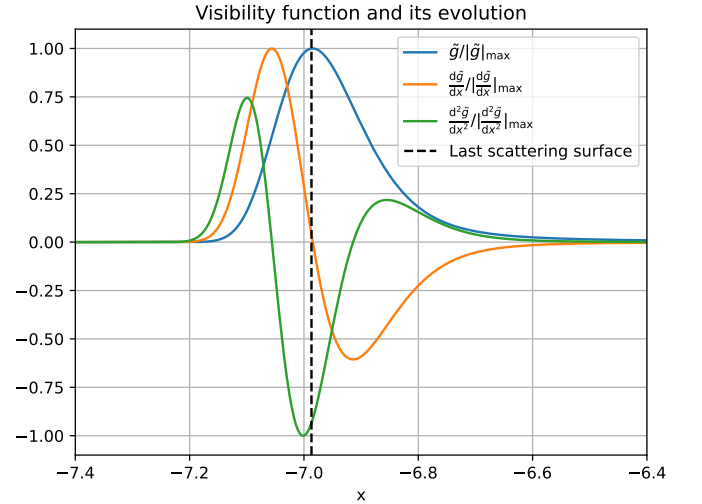

Fig. 12. Plot showing the visibility function ($\tilde{g}$) and its two first derivatives.

Figure 12 shows the visibility function and its derivatives. The visibility function and its derivatives have been scaled to fit into the same plot, with the first and second derivative having much larger values than the visibility function it self. The visibility function describes the probability that a observed photon was last scattered at time x, going backwards in time from today. In Figure 12 it can be seen that this probability is

---

[22] Note that if only the Saha approximation is used, we will be half way through recombination at $x = -7.230$.

more or less zero both before and after recombination. This can be understood as a dense and opaque Universe before recombination, where photons scattered constantly, and thus the probability of a photon observed today scattered last time before recombination is almost zero. After recombination the Universe is transparent, huge and "empty". Here Thompson's scattering rate is lower than the expansion's, as $\tau' < 1$, and so the chance for scattering is really low.

The sound horizon at decoupling has also been computed, being this $r_s \approx 128.177$ Mpc.

4.3. Solving the evolution of structure in the Universe

For all the main physical quantities in this subsection, four different scales, or wave numbers, are presented. The values are selected in order to display solutions from each type of scale-regime:

– Large scales, entering early in the radiation dominated regime, with small wave numbers; $k = 0.001$ Mpc^{-1} and $k = 0.0001$ Mpc^{-1}.
– Intermediate scales, entering right before and after radiation-matter-equality, with $k = 0.01$ Mpc^{-1}.
– Small scales, entering early in the radiation dominated regime, with a large wave number, $k = 0.1$ Mpc^{-1}.

In Figure 13 one can see the density perturbations for baryonic (ordinary) matter, cold dark matter and photons. First interpreting the pressure-less CDM which is able to start growing, it can be seen that the perturbations on all scales remain constant until gravity can start contracting them, due to entering the horizon and thus becoming causally connected.
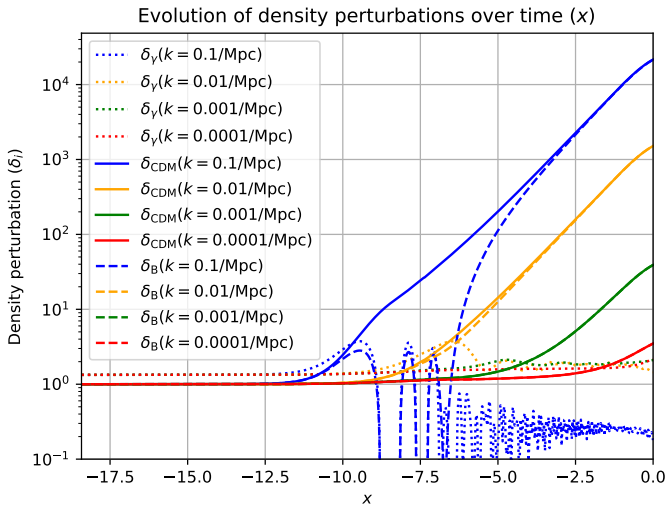

Fig. 13. Density perturbations for baryonic matter (δ_B), cold dark matter (δ_{CDM}) and photons (δ_γ) over time (x).

Looking at the baryonic perturbations much of the same behavior can be seen, with the only exception being scales entering the horizon before the end of recombination not growing beyond a certain value, but instead oscillating. This is due to their tight coupling with the photons and the early baryon-photon fluid. This will be evident in the photon perturbations. The equations for the perturbations can be expressed on the form of a driven harmonic oscillator, with gravity being the attracting force and radiation pressure the repulsive force. This balance will cause the baryonic perturbations, entering before the decoupling of the baryons and photons, to oscillate, first being compressed when the gravitational force is dominating before the radiation pressure starts to dominate. The large scale perturbations, entering after recombination is not affected by this coupled state, and will not oscillate but just follow the dark matter perturbations. This effect is clearly visible on the small scales, oscillating heavily until the end of recombination. At this point the baryons are not coupled to the photons any more, and are free to fall into and follow the large gravitational potential wells set up by the dark matter perturbations. On the intermediate scales, a minor effect of this radiation pressure can be seen, causing a slight delay on the baryons growth relative to the CDM, before catching up again.

For the photon perturbations much of the same behavior is seen, as for the baryon perturbations before recombination, due to their tight coupling. The perturbations are constant before entering the horizon. The small scales that enter early start oscillating heavily together with the baryons, with the oscillations being dampened onward in time until decoupling after recombination. After decoupling, the optical depth has dropped significantly, and the photons are free to move more or less unhindered and no longer collapses together with the baryons. The dampening of the harmonic oscillations cause the perturbations to eventually be more or less constant, until the dark energy dominated regime when expansion causes them to start decay to zero. The intermediate scales are barely affected by the coupled oscillated regime, and undergoes only a single peak before decoupling, while the large scales enter well into the matter dominated regime and is not affected by the coupling.

In Figure 14 one can see the velocity perturbations for baryonic (ordinary) matter, cold dark matter and photons. The velocities of the CDM perturbations increase from close to zero until horizon entry, consistent with the horizon being bigger and bigger and thus the part of the causally connected mass within increasing, pulling more and more, so that the matter falls gradually faster and faster.

The baryonic matter velocities follow the oscillations, but with a phase shift of $\pi/2$ so that the minimum value of the velocity corresponds to the maximum size of the perturbation, and vise versa, consistent with the harmonic oscillator description. For both the densities and the velocities it can be seen how the early oscillations are dampened over time closer to recombination, due to diffusion dampening caused by the mean free path of the photons increasing with the decreasing optical depth.

Again, it can be seen that the photon velocities are following the density in a similar fashion as for the baryons, being phase shifted by $\pi/2$.

In Figure 15 the photon quadrupoles can be seen, related with the polarization source, which will be relevant in a future work.

Lastly, the gravitational potentials are presented in Figure 16. Here it is evident that $\Psi \approx -\Phi$, and thus we will keep to discussing Φ alone where it is inferred that Ψ behaves similarly. Again are all scales constant before entering the horizon, and
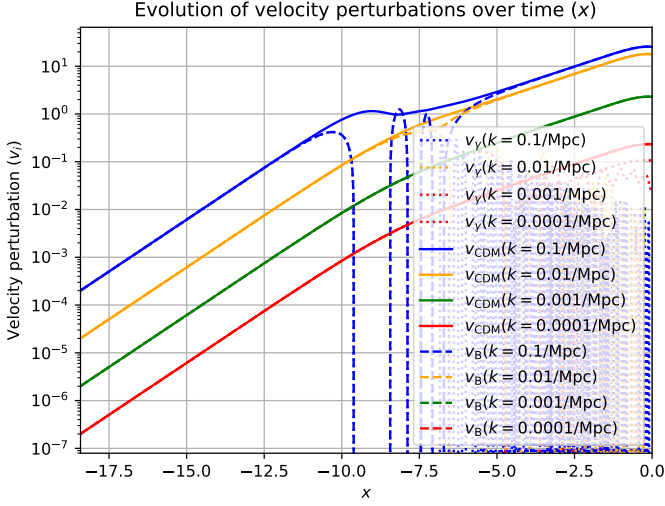
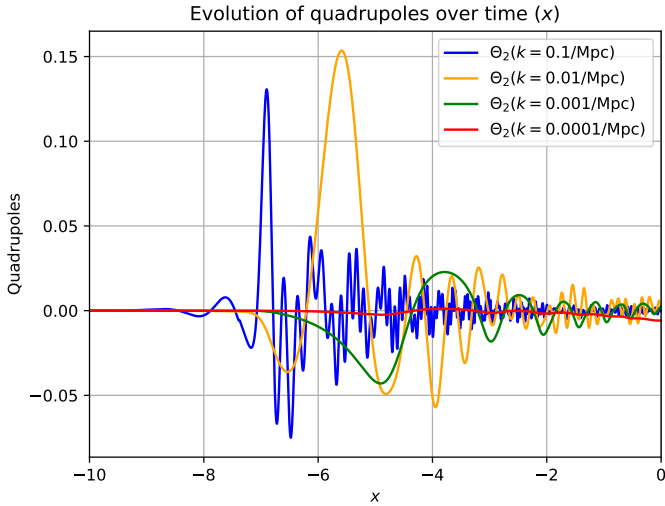**Fig. 14.** Velocity perturbations for baryonic matter (v_B), cold dark matter (v_{CDM}) and photons (v_γ) over time (x).

Fig. 16. Evolution of potentials over time (x).

Fig. 15. Photon quadrupole perturbations over time (x).

For the intermediate scales we see the slight effect of the one oscillation of the monopole before the matter perturbations are too dominating, resulting in a minor drop off from the initial value, flattening out after recombination. The largest scales entering well inside the matter dominated regime are nearly unaffected from their initial conditions, and it can be shown to drop of by a factor of 9/10 into the matter dominated regime, which is consistent with the way our solutions for how the large scales behave. Note that the potentials all starts to decay into the dark energy regime, where expansion causes even the largest potentials to be smoothed out.

4.4. Computing the CMB power-spectrum

In Figure 17 displays the resulting multipoles obtained from Equation **??** through the line of sight integration method, for four significantly different angular scales in the studied interval. Here it can be seen the oscillatory and dampening effect from the Bessel functions, as the transfer functions look like damped harmonic oscillators.

The integrand from Equation **??** is shown in Figure 18. As it shows essentially the square of the transfer function, one will expect to see much of the same trends, with only positive values, with the larger scales even more dominant as it is divided by the wavenumber. However, this is not the case, from where one could infer that there has to be some kind of mistake in the code. Here it could be expected to see how the different scales will affect the power spectrum in the end, and which wavenumbers contributes to the different angular scales. As $k \sim \ell/\eta_0$ this is not so surprising, seeing that the larger scales, low ℓ, have a contribution on small k, and vice versa.

In Figure 19 the total matter power-spectrum can be seen. For large scales perturbations, it can be seen how the late horizon entry and hence being affected by little causal physics, results in a more or less unprocessed perturbations. Seeing a scale dependence consistent with initial perturbations being set up by a Gaussian random field, where more perturbations of "medium" scale and less of the super-horizon scales are expected, it results in the spectrum proportional to k^{n_s}, where

behaves quite differently depending on the time of entry.

In our understanding of these gravitational potentials we think of them as a type of Newtonian potential. On small scales, entering the horizon and being causally connected in the radiation dominated regime, the potentials are dominated by radiation energy, which does not cluster efficiently. Thus the potentials decay rapidly when the monopole increases, but start to oscillate due to the baryon-photon-fluid oscillations until after decoupling.

When entering into the matter dominated regime, the dominating energy contributor to the potentials are baryons and the CDM, which do indeed cluster and causes the potentials to be constant with growing matter perturbations. The larger scales have less time to collapse, as can be seen in the difference between the small scales, and thus holds a larger constant value through the matter dominated regime.
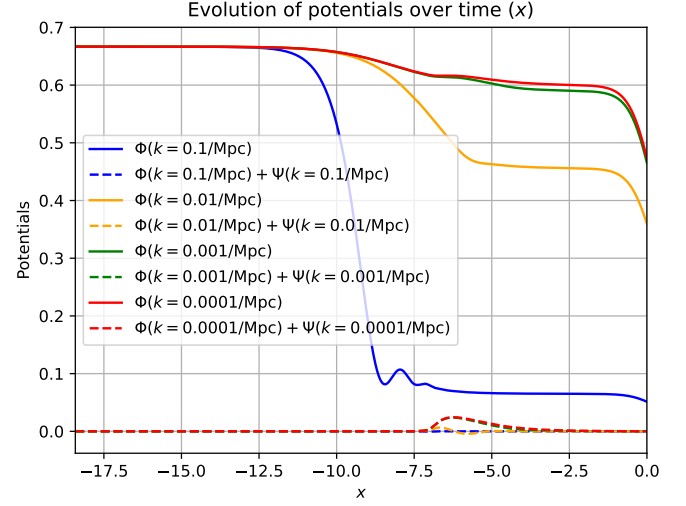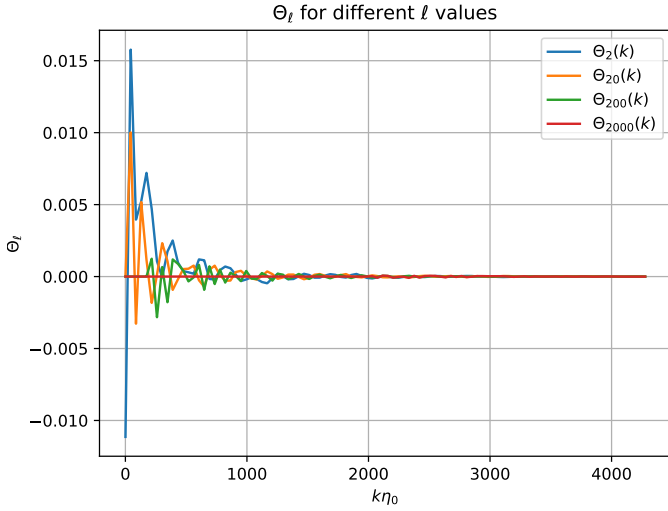
Fig. 17. Transfer function Θ_ℓ obtained from line of sight integration in Equation **??** for four different ℓ's.

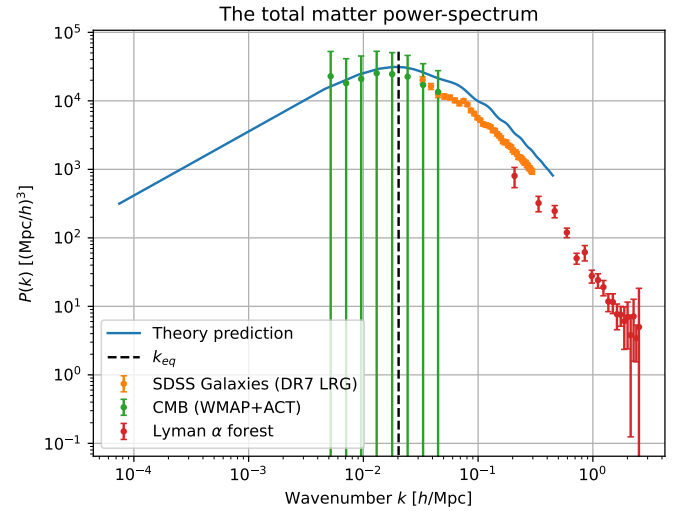**Fig. 18.** The integrand Θ_ℓ Equation **??** for four different ℓ's.

Fig. 19. The matter power spectrum, with the equality scaled (k_{eq}) marked in as the vertical dotted line. For larger scales the spectrum goes as $k^{n_s} \sim k^1$, while small scales being suppressed by the Meszaros effect going as k^{n_s-4}, being suppressed by k^{-4} relative to the larger scales entering after matter-radiation equality.
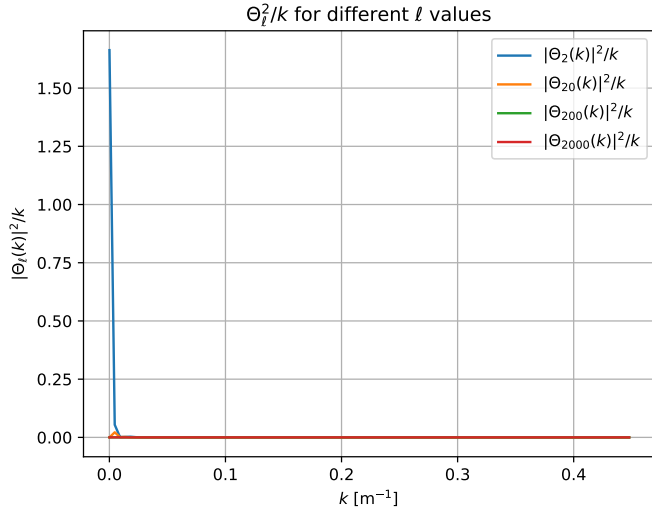
the spectral index n_s is close to unity, being determined by the length of the inflationary period.

Going to smaller scales the peak in the spectrum is hit, at the equality scale k_{eq}. This is the scale corresponding to perturbations entering the horizon at the matter-radiation equality. The matter perturbations grows differently with time in the matter and radiation era, and also when being outside and inside the horizon.

The main result, the CMB power spectrum, is shown in Figure 20. Reading the plot from large scales to small, we see the plateau on the largest scales, with the late ISW effect contributing to the increase on the very largest scales in $\ell \lesssim 10$. This is due to the dark energy dominated regime, where the accelerated expansion halts the growing modes and thus the derivatives of the gravitational potentials are large. Increasing the dark energy density parameter would cause the dark energy

to dominate earlier, and we would have a larger late ISW effect.

Moving on, the first peak, called the acoustic peak, can be found. This is a remnant from the tight coupled regime between baryons and photons in the early perturbations. The baryon-photon fluid traveling as one in the tight coupled regime, before the photons decouple leaving the baryons behind. The baryons are then affected by the gravity of dark matter perturbations, and the baryons affecting the dark matter. The result is a high peak at the $\ell \sim 200$ scale.

On the smaller scales it can be seen how the power spectrum starts to oscillate, called acoustic oscillations, and eventually being exponentially suppressed. Looking at the monopole oscillations from the previous subsection the oscillations can be understood. The equation for the monopole can be characterized as a driven harmonic oscillator. The peaks in the C_ℓ corresponds to scales for which the effective monopole oscillations have a maximum or minimum at the time of recombination, or at the last scattering surface (LSS). The troughs in the power spectrum corresponds to scales where the effective monopole is zero at LSS. The photon perturbations characterized by the driven harmonic oscillator equation can be thought of as a simple mass less ball on a spring in a gravitational field, oscillating up and down in a driven motion. If photon perturbations were considered, these oscillations would have been even around the zero point. But as the baryon and photons are heavily coupled, and the baryons having mass in the gravitational field, we can instead think of the oscillator as a ball on a spring, but with mass. The oscillations being due to the balance between gravity and radiation pressure, adding the baryons with mass enhances the compression modes, but not so much the rarification. Thus we get an uneven oscillation, every compression being enhanced, which corresponds to the odd numbered peaks in the power spectrum. This we can clearly see in Figure 20, where the first and third peak being larger than the second and fourth and so on. For higher number peaks this is harder to make out, as the exponential suppression of the power spectrum kicks in.

This gives us another insight into determining the cosmological parameters. Measuring the relative height of the even and odd numbered peaks we can infer restrictions on the baryon density parameter.

Lastly, the exponential suppression on the smallest scales can be seen. This effect is due to photon diffusion, caused by the photons moving in a so called random walk motion through the photon-baryon fluid due to the photons scattering on the free electrons. The average distance the photons travel between each scattering is called the mean free path, λ_{mfp}, being dependent on the free electron density. Following the central limit theorem, after n scatterings the photons would have moved on average a distance $\lambda_D \sim \sqrt{n}\lambda_{\mathrm{mfp}} \sim 1/\sqrt{n_e \sigma_T H}$. or perturbations on scales smaller than this distance, the over- and underdensities are able to mix dampening the oscillations. This effect is especially prominent for scales for which the finite thickness of the LSS is not negligible relative perturbation size. This is called diffusion dampening, or silk dampening, exponentially suppressing the anisotropies on scales $\ell \lesssim 500$. This effect is also dependent on the baryon density parameter because of the scattering, as well as the helium fraction and the number of relativistic particles in our Universe. The latter being determined by the number of massless neutrinos.
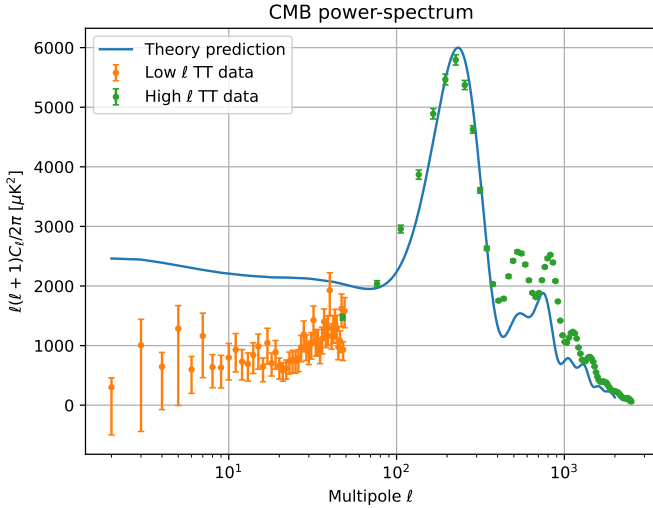

Fig. 21. Contribution of each term to the final CMB power-spectrum

Fig. 22. Contribution of each term to the final CMB power-spectrum from Baumann (2018).

Fig. 20. CMB power-spectrum with the observational data.

In Figure 21, the contribution of each term to the final CMB power-spectrum can bee seen. Comparing with Figure 6 in Baumann (2018) (Figure 22 in this work) one can see that there is a discrepancy in the Doppler term, possibly being this the reason why there is a discrepancy between the computed CMB power-spectrum and the observational data plotted in Figure 20.

Additionally, a map of the CMB power-spectrum as been generated, being shown in Figure 23.

Fig. 23. CMB map generated using Healpy.

5. Conclusions

Background cosmology of the Universe has been solved and each epoch has been determined, identifying in each of them the dominating substance. The age of the Universe has also been
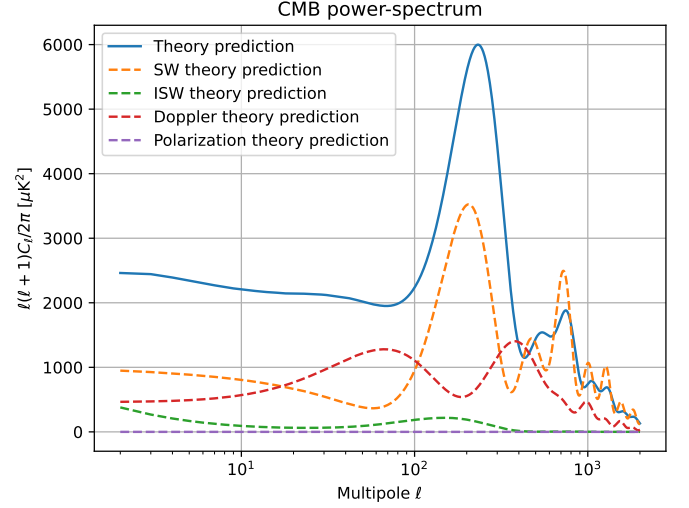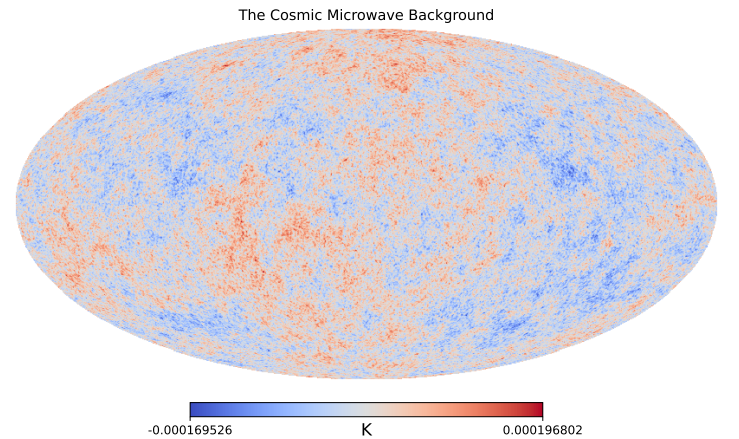
computed, being this $t_{\mathrm{Universe}} \approx 13.86$ Gyr.

Recombination history of the Universe has been solved, computing different important times during recombination, summarized in Table 3. The sound horizon at decoupling has

also been computed, being this $r_s \approx 128.177$ Mpc.

The evolution of the structure in the Universe has been solved and the different kind of perturbations have been determined, showing that the metric in our Universe deviates from the Friedmann-Lemaître-Robertson-Walker (FLWR), implying that our Universe is not homogeneous nor isotropic.

The matter and CMB power-spectra have been computed with high accuracy, except for the low ℓ's in the CMB power-spectrum due to some mistake in the Doppler term of the source function.

References

Aghanim, N., Akrami, Y., Ashdown, M., et al. 2020, Astronomy amp; Astrophysics, 641, A6

Baumann, D. 2018, 009

Betoule, M., Kessler, R., Guy, J., et al. 2014, Astronomy amp; Astrophysics, 568, A22

Callin, P. 2006, How to calculate the CMB spectrum

Dodelson, S. 2003, Modern Cosmology (Academic Press, Elsevier Science)

Seljak, U. & Zaldarriaga, M. 1996, The Astrophysical Journal, 469, 437